International Journal of Heat and Mass Transfer 52 (2009) 4095–4102

Contents lists available at ScienceDirect

International Journal of Heat and Mass Transfer

journal homepage: www.elsevier.com/locate/ijhmt

Numerical simulation for natural convection in vertical channels

Xiuling Wang [a], Darrell W. Pepper [b,*]

[a] Department of Mechanical Engineering, Purdue University Calumet, Hammond, IN 46323, USA
[b] Department of Mechanical Engineering, University of Nevada Las Vegas, Las Vegas, NV 89154, USA

ARTICLE INFO

Article history:
Received 17 November 2008
Accepted 23 March 2009
Available online 7 May 2009

Keywords:
Natural convection
Vertical channel
h-Adaptive finite element method

ABSTRACT

The investigation of laminar natural convection in vertical obstructed channels is conducted using an *h*-adaptive finite element algorithm. The adaptive model uses an L_2 norm based *a-posteriori* error estimator with a semi-implicit, time-stepping projection technique. The advection terms are treated using an explicit Adams Bashforth method while the diffusion terms are advanced by an implicit Euler scheme. By using the adaptive algorithm, mesh independent studies can be avoided. Results are obtained for thermal and flow patterns including average Nusselt numbers for different parameters (Rayleigh number, aspect ratio and locations of obstructions) in both smooth and obstructed channels.

1. Introduction

Natural convection flows in vertical channels with obstructions can be found in many engineering applications, e.g., heat exchangers, heat transfer in electric circuits and energy storage systems. Considerable experimental work as well as many numerical simulations has been carried on for many years in this area [1–9,15].

From a numerical aspect, much of the early numerical work stems from the techniques advocated by Spalding [11] and his students during the 1960s and early 1970s. Burch et al. [6] investigated the laminar natural convection between finitely conducting vertical plates by a finite-difference procedure. Said and Krane [5] investigated laminar natural convection flow of air in a vertical channel with a single obstruction numerically, using a set of finite element codes initially developed by Gartling [17]. Desrayaud and Fichera [7] simulated natural convection in a vertical isothermal channel with two rectangular ribs, symmetrically located on each wall. They used the SIMPLER algorithm [16], based on the initial pressure-based finite volume method technique described by Patankar [16], a former student of Spalding.

Generally when conducting natural convection simulation studies, a mesh independent study is typically needed for higher Ra values; these studies can become time consuming and costly. An alternative way to avoid this procedure is to apply adaptive meshing [12]. Many commercial CFD codes today now employ some form of low-level adaptive meshing. In this study, a locally *h*-adaptive mesh refinement algorithm is coupled with a Petrov–Galerkin finite element method (PFEM). Meshes are refined in regions where flow features change rapidly and coarsened where the flow properties are smooth and unvarying. The adaptation procedure is guided by an L_2 norm based *a posterior* error estimator. A semi-implicit, time-stepping projection technique is used for the flow solver. A more detailed description of the projection method is discussed in Ramaswamy et al. [10] and Wang and Pepper [13].

Simulation results for natural convection in a vertical channel are obtained first without any obstructions. A channel with one obstruction is then examined, followed by a channel with two obstructions. Thermal and flow patterns are obtained for different Rayleigh numbers, channel aspect ratios and obstruction locations. Results are compared with those obtained by Said and Krane [5] for natural convection in a vertical channel with one obstruction. Results for natural convection within a vertical channel with multiple obstructions are compared with experimental values obtained by Cruchaga and Celentano [2].

2. Governing equations and finite element formulation

The following non-dimensional relations are defined (non-dimensional terms are labeled with "*") for the governing equations of 2-D, incompressible fluid flows with natural convection effects (Boussinesq approximation and constant fluid properties are adopted):

$$x^* = \frac{x}{a},\ y^* = \frac{y}{L},\ r^* = \frac{r}{L},\ u^* = \frac{u}{\alpha/a},\ v^* = \frac{v}{\alpha/L},\\ P^* = \frac{P}{\rho\alpha^2/L^2},\ \theta^* = \frac{T-T_\infty}{T_w-T_\infty} \tag{1}$$

The corresponding non-dimensional conservation equations can be written as (after dropping the asterisks for convenience).

* Corresponding author.
E-mail address: dwpepper@nscee.edu (D.W. Pepper).

0017-9310/$ - see front matter © 2009 Elsevier Ltd. All rights reserved.
doi:10.1016/j.ijheatmasstransfer.2009.03.045

Nomenclature

a	channel width
Ar	aspect ratio of the channel, b/L
e	error
$\bar{e}_{avg}$	average element error
L	channel height
L_1	distance to the obstruction on the left side wall from the entrance of the channel
L_2	distance to the obstruction on the right side wall from the entrance of the channel
m	total element number
N_i	shape function
P	pressure
Pr	Prandtl number
r	radius of obstruction
Ra	Rayleigh number
t	time
T	temperature
T_w	wall temperature
T_∞	ambient temperature
u,v	velocity components in x and y direction

Greek symbols

$\overline{\alpha}$	Petrov–Galerkin weighting function
α	thermal diffusivity
β	thermal expansion coefficient
θ	non-dimensional temperature $(T - T_w)/(T_w - T_\infty)$
μ	dynamic viscosity
ν	kinematic viscosity
ρ	density
ξ_i	adaptation indicator
η	error index
$\bar{\eta}_{\max}$	maximum specified error

Conservation of mass

$$\frac{\partial u}{\partial x}+\frac{\partial v}{\partial y}=0 \tag{2}$$

Conservation of momentum
x-direction:

$$\frac{\partial u}{\partial t}+u\frac{\partial u}{\partial x}+v\frac{\partial v}{\partial y}=-\nabla p+\Pr\left(\frac{\partial^2 u}{\partial x^2}+Ar^2\frac{\partial^2 u}{\partial y^2}\right) \tag{3}$$

y-direction:

$$\frac{\partial v}{\partial t}+u\frac{\partial u}{\partial x}+v\frac{\partial v}{\partial y}=-\nabla p+\Pr\left(\frac{\partial^2 v}{\partial x^2}+Ar^2\frac{\partial^2 v}{\partial y^2}\right)+Ra\Pr Ar\theta \tag{4}$$

Conservation of energy

$$\frac{\partial \theta}{\partial t}+u\frac{\partial \theta}{\partial x}+v\frac{\partial \theta}{\partial y}=\frac{\partial^2 \theta}{\partial x^2}+Ar^2\frac{\partial^2 \theta}{\partial y^2} \tag{5}$$

with the Rayleigh and Prandtl numbers defined as

$$Ra=\frac{g\beta(T_w-T_\infty)b^3}{\alpha v},\ \Pr=\frac{v}{\alpha} \tag{6}$$

Bilinear quadrilateral elements are chosen in a Petrov–Galerkin weighted residual finite element approach (PFEM) to discretize the problem domains. The variables u, v and θ are replaced by using the trial functions

$$u(x,y,t)=\sum_{i=1}^{n}N_i(x,y)u_i(t) \tag{7}$$

$$v(x,y,t)=\sum_{i=1}^{n}N_i(x,y)v_i(t) \tag{8}$$

$$\theta(x,y,t)=\sum_{i=1}^{n}N_i(x,y)\theta_i(t) \tag{9}$$

The matrix equivalent form of the integral-based finite element equations can be expressed as

$$[M]\{\dot{V}\}+([K]+[A(V)])\{V\}=\{F_V\} \tag{10}$$

$$[M]\{\dot{\theta}\}+([K_\theta]+[A(V)])\{\theta\}=\{F_\theta\} \tag{11}$$

where a Petrov–Galerkin approximation is employed to assist in the discretization of the advection terms associated with velocity and temperature transport, i.e.,

$$W_i=N_i+\frac{\overline{\alpha}h_e}{2|V|}[V\nabla N_i] \tag{12}$$

where $\overline{\alpha}=\coth\frac{\gamma}{2}-\frac{2}{\gamma}$. A detailed description of the matrix relations and formalization of the numerical algorithm is described in Wang and Pepper [13].

3. Adaptation technology

The finite element method has been widely used in various engineering analysis areas for many decades. In particular, the use of adaptive techniques with the finite element method has resulted in accurate simulation results with overall reduced computational storage and solution times. The most popular CFD codes today employ some form of mesh adaptation.

In this study, an h-adaptive PFEM approach was selected to solve for fluid flow with convective heat transfer effects. An *a-posteriori* error estimator based on L_2 norm error calculation is adopted to guide the adaptation procedure [13].

A local element refinement indicator is defined to decide if a local refinement for an element is needed, i.e.

$$\xi_i=\frac{\|e\|_i}{\bar{e}_{avg}} \tag{13}$$

when $\xi_i>1$, the element is refined; when $\xi_i<1$ the element is coarsed. In an h-adaptive process, the new element size can be calculated by:

$$h_{new}=\frac{h_{old}}{\xi_i} \tag{14}$$

The entire adaptation procedure is shown in Fig. 1.

A more detailed discussion of the h-adaptive PFEM technique along with the error estimator as employed in this study is given in Pepper and Wang [14]. Additional work on the development and implementation of p- and hp-adaptation is described in Wang and Pepper [13].

4. Numerical simulations

4.1. Natural convection in a smooth channel

Natural convection in a smooth vertical channel was simulated as a first comparison study for an obstructed channel flow. Problem geometry and boundary conditions are shown in Fig. 2. The left and right walls are kept at high temperature, while the inlet is kept at a constant low temperature. The horizontal velocity is zero at the inlet. Both inlet and outlet pressures are also kept at zero.

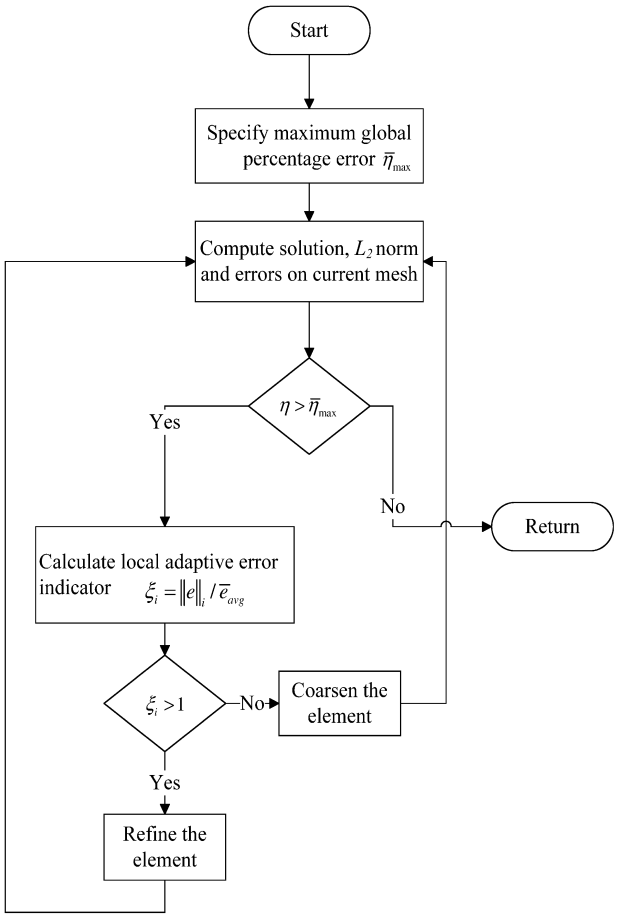

Fig. 1. Flow chart for adaptation procedure.

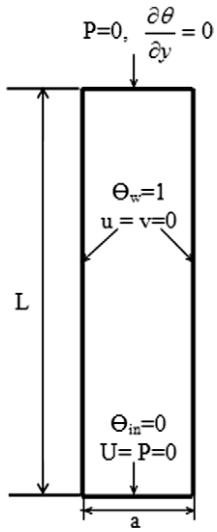

Fig. 2. Boundary conditions and initial mesh for smooth channel.

Results were obtained for Rayleigh numbers ranging from 10^2 to 10^5 and Ar = 0.2. Good agreement with data in the literature was observed over the range of Rayleigh numbers considered. Isotherms are shown in Fig. 3 for Ra = 10^2, 10^3, 10^4, and 10^5, respectively. The Isotherms range from 0 to 1 with 0.1 as the contour interval.

Fig. 3 shows that as Ra increases, convective heat transfer effects begin to dominate from the entrance of the channel to

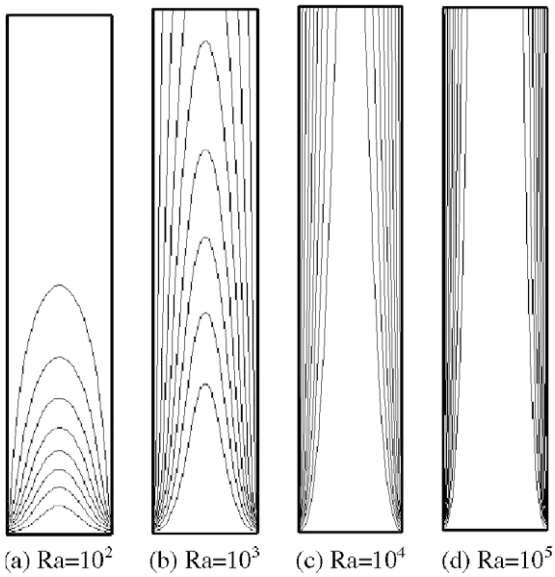

Fig. 3. Isotherms for natural convection in smooth channel.

eventually over the entire length of the channel. The thermal boundary layer thickness also begins to thin along the vertical walls, as expected with increasing flow velocity and Rayleigh number.

The initial computational mesh consisted of 441 elements for all the Rayleigh numbers. The final *h*-adaptive FEM meshes are shown in Fig. 4 for the different Rayleigh numbers. The mesh becomes refined within the boundary layer; this is due to computational errors that develop as a result of the large gradients that occur along the walls. After four levels of *h*-adaptation, the total number of elements is: 3514 (Ra = 10^2), 2788 (Ra = 10^3), 2299 (Ra = 10^4), and 2518 (Ra = 10^5), respectively.

Local Nusselt numbers versus distance along the vertical channel walls are shown in Fig. 5. The definition for local Nusselt number is:

$$Nu_y = a\nabla T \cdot n \tag{15}$$

As the Rayleigh number increases, the magnitudes of local Nusselt numbers increase as a result of the enhanced convective heat transfer effects and larger temperature gradient in near wall

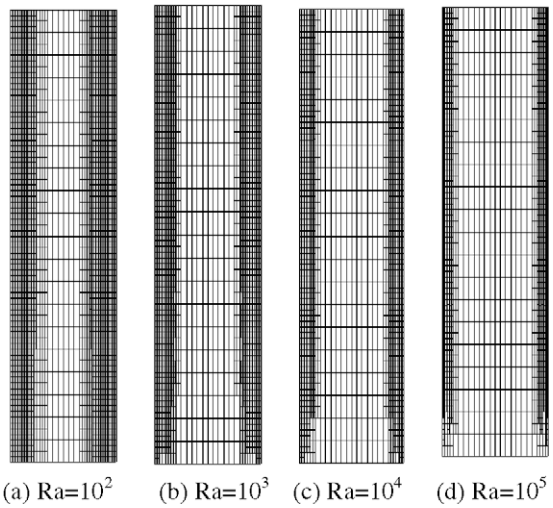

Fig. 4. Adapted meshes for smooth vertical channel.

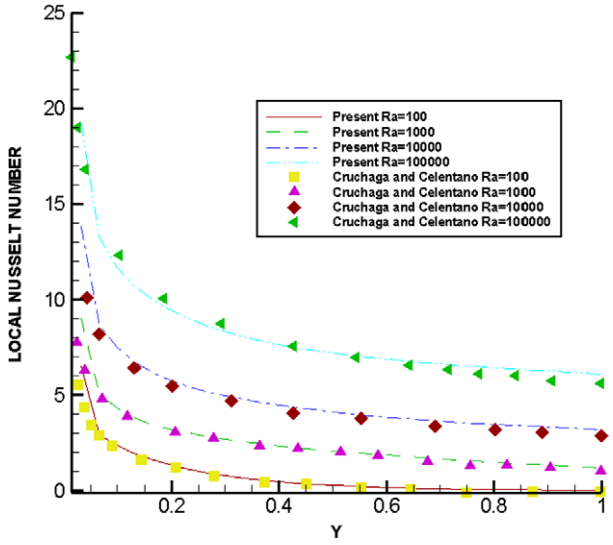

Fig. 5. Local Nusselt number along vertical walls.

regions. The local Nusselt number decreases rapidly near the entrance of the channel and then decays slowly as the flow reaches the upper region of the wall. Comparison of the present results for local Nusselt numbers is also shown in Fig. 5. Close agreement can be observed with computational results obtained by Cruchaga and Celentano [2].

4.2. Natural convection in a vertical channel with one obstruction

To study the effects of obstruction in the vertical channel, a single obstructed channel is first considered. Boundary conditions for a vertical channel with a circular obstruction at the middle of its height are shown in Fig. 6. The circular obstruction lies in the middle of the left vertical wall, with radius 0.091, with both left and right walls kept at high temperatures. Aspect ratio Ar = 0.2727 and Ra = 2×10^4 were chosen, and results compared with experimental and numerical data obtained by Said and Krane [5].

Isotherms and streamlines are shown in Fig. 7. The streamlines around the obstruction are getting tight, which show that air is accelerating as a result of the sudden change in cross sectional area. The velocity increases accordingly.

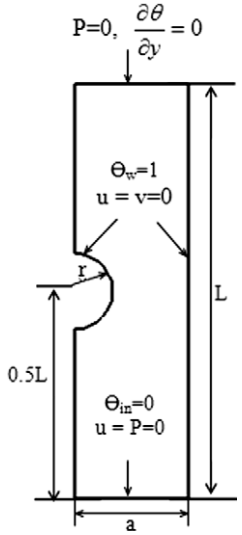

Fig. 6. Boundary conditions for vertical channel with single obstruction.

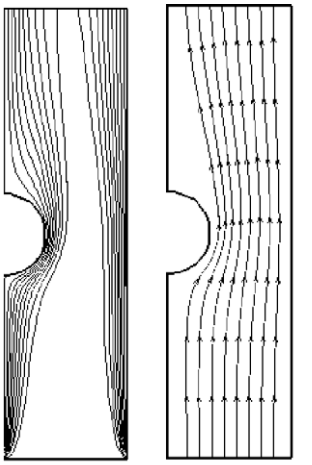

Fig. 7. Results for natural convection in vertical channel with one obstruction.

Computational meshes are shown in Fig. 8. Fig. 8(a) shows the initial mesh with 710 elements and 786 nodes. The final adapted mesh, shown in Fig. 8(b), contains 4616 elements with 4557 nodes. The mesh is refined around the obstruction and within the boundary layers. In this case, four levels of refinement were undertaken.

As expected, the flow accelerates around the obstruction. As seen in the final adapted mesh, elements become refined and clustered in regions where the flow is rapidly changing and the error is large. One of the advantages of using adapted meshing is that the final mesh acts as a very good indicator of those regions where most of the computational effort is being made.

To quantitatively compare the simulation results with data found in the literature, the distribution of vertical velocity and temperature profiles are presented in Fig. 9(a and b). Fairly close agreement can be observed between the present results and the experimental values from Said and Krane [5].

4.3. Natural convection in a vertical channel with multiple obstructions

Natural convection in a vertical channel with multiple obstructions on parallel walls is finally examined. In this third set of

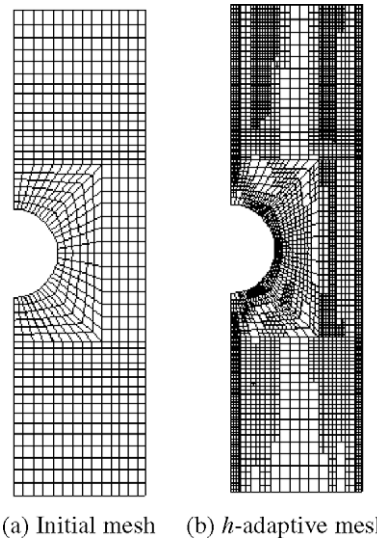

Fig. 8. Computational mesh for vertical channel with single obstruction.

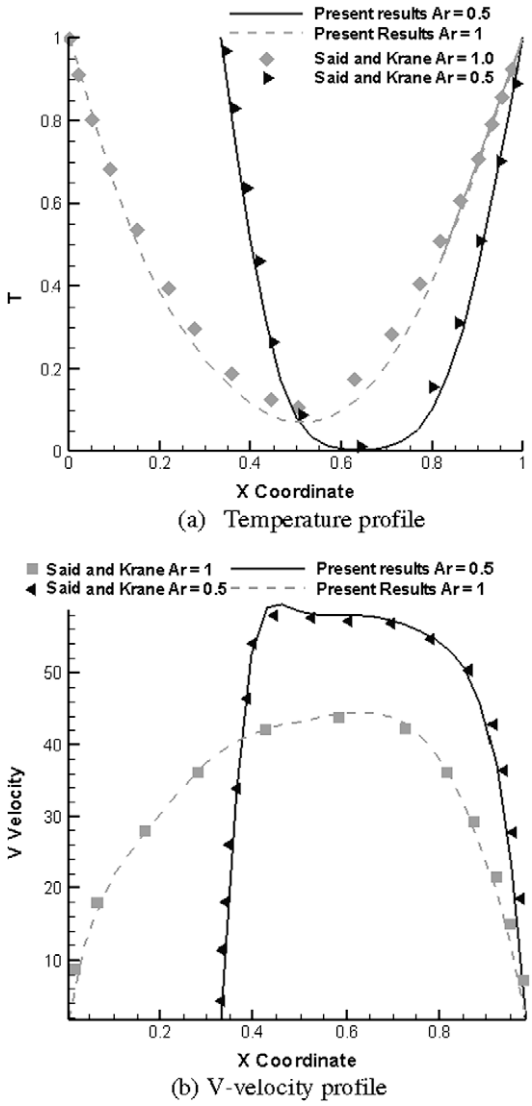

Fig. 9. Temperature and vertical velocity profile for vertical channel with single obstruction.

simulations, two obstructions are selected to demonstrate the effects on the natural convection patterns. While additional obstructions can be added, the evolving flow and thermal patterns as a result of adding more obstructions are fairly straightforward. The problem definition is shown in Fig. 10. In the vertical channel, both the left and right walls (including the obstructions) are heated. The inlet is kept cool, with the horizontal velocity set to zero. Both the inlet and outlet pressures (nondimensional) are set to zero.

Simulations were conducted considering various effective factors: Rayleigh number, aspect ratio of the channel and the location of the obstructions. The two obstructions are the same size for all cases with the width set to 0.0667L and the height equal to 0.01334L. The Rayleigh number varied from 10^2 to 10^5. The characteristic lengths for the different test cases are listed in Table 1.

Flow and thermal patterns were obtained and the results compared for the different Rayleigh number settings. Figs. 11 and 12 show the temperature and fluid velocity patterns for setting 1 at various Rayleigh numbers. Notice that as the Rayleigh number increases, natural convection becomes more enhanced with the recirculation regions downstream of the obstructions becoming more amplified. The boundary layer thickness decreases due to the increase in convection effects, as seen in Fig. 11. The isotherms are plotted using 0.1 intervals.

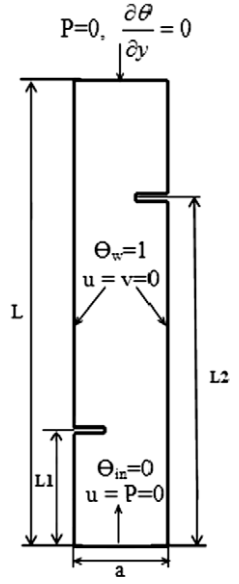

Fig. 10. Boundary conditions for vertical channel with two rectangular obstructions.

Table 1
Summary of characteristic length.

	Ar (a/L)	L_1/L	L_2/L
Setting 1	0.2	0.25	0.75
Setting 2	0.2	0.5	0.5
Setting 3	0.3	0.25	0.75
Setting 4	0.3	0.5	0.5

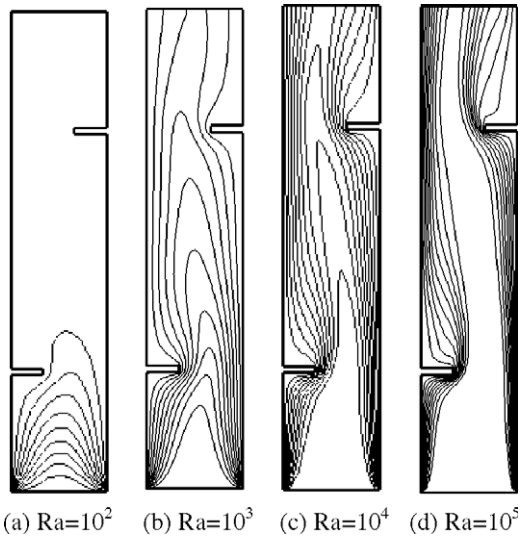

Fig. 11. Isotherms for natural convection in vertical channel with two obstructions (setting 1).

At the locations of the obstructions, streamlines become tightened, as seen in Fig. 12, and indicate the existence of sudden changes in the flow, i.e., the flow accelerates.

The adaptive meshes for the different Rayleigh numbers are shown in Fig. 13. The meshes are especially refined in the boundary layer regions and around the obstructions, and correlate with those regions where the fluid velocities and temperatures are changing rapidly. These mesh refinements can be directly linked to areas

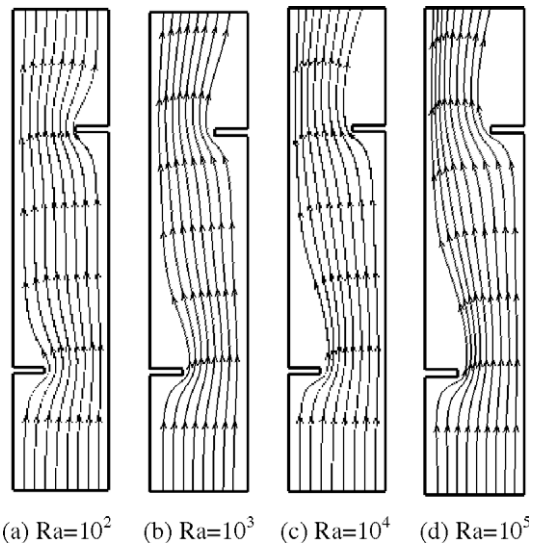

Fig. 12. Streamlines for natural convection in vertical channel with two obstructions (setting 1).

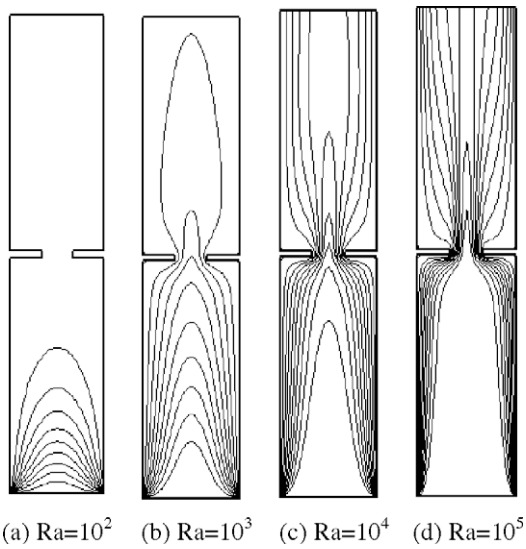

Fig. 14. Isotherms for natural convection in vertical channel with two obstructions (setting 2).

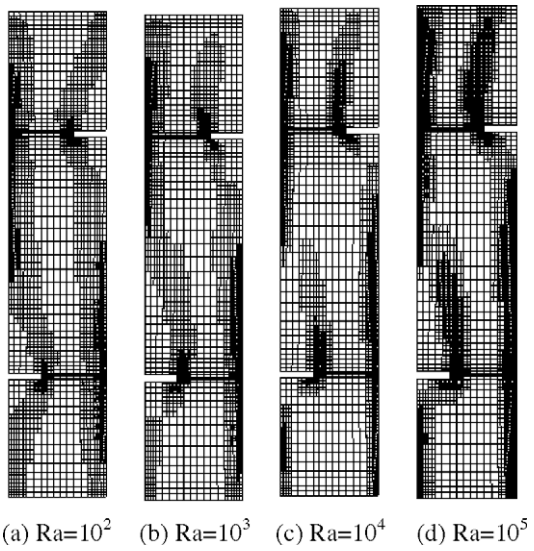

Fig. 13. Adaptive meshes for natural convection in vertical channel with two obstructions (setting 1).

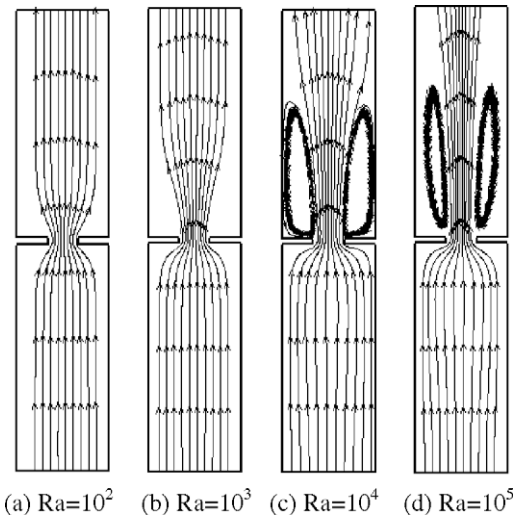

Fig. 15. Streamlines for natural convection in vertical channel with two obstructions (setting 2).

of large computational error. As the Rayleigh number continues to increase, the boundary layers become thinner, with the adaptive meshes becoming more clustered near the walls and around obstructions as well. Results were also obtained for natural convection in a vertical channel with obstructions located symmetrically on opposite walls. The corresponding isotherms and streamlines are shown in Figs. 14 and 15.

Comparing the isotherms in Fig. 14 with those in Fig. 11 at the same Rayleigh number, it is apparent that the convective heat transfer effects are stronger when the obstructions are not symmetrically located. This can be explained by comparing the streamlines in Fig. 15 with those in Fig. 12. When the obstructions are symmetrically placed in the channel, the recirculation regions are much larger, leading to more enhanced mixing which substantially reduces the total heat transfer for this geometry.

The average Nusselt number comparisons for vertical channels with aspect ratio 0.2 are shown in Fig. 16 with obstructions at different locations. It is observed that the average Nusselt number is higher for setting 1 (where one obstruction is closer to the entrance of the channel while the other obstruction has been moved more towards the exit of the channel) than for setting 2 (where obstructions are symmetrically located in the channel). This difference is attributed to the reduced heat transfer associated with the larger recirculation zones. The average Nusselt number is in agreement with computational values obtained by Cruchaga and Celentano [2].

Figs. 17–20 show simulation results with different channel aspect ratios. With obstructions set at same locations as settings 1 and 3, similar patterns occur in both the fluid flow and thermal patterns (see Fig. 11 vs. Fig. 17; Fig. 12 vs. Fig. 18). The similarities were also observed for settings 2 and 4 (Fig. 14 vs. Fig. 19; Fig. 15 vs. Fig. 20).

Even though the thermal and fluid flow patterns appear similar when obstructions are located at the same positions with different channel aspect ratios, the heat transfer effect becomes more dramatic as the aspect ratio is increased. This can be seen at especially high Rayleigh numbers, e.g. Fig. 14(d) vs. Fig. 19(d).

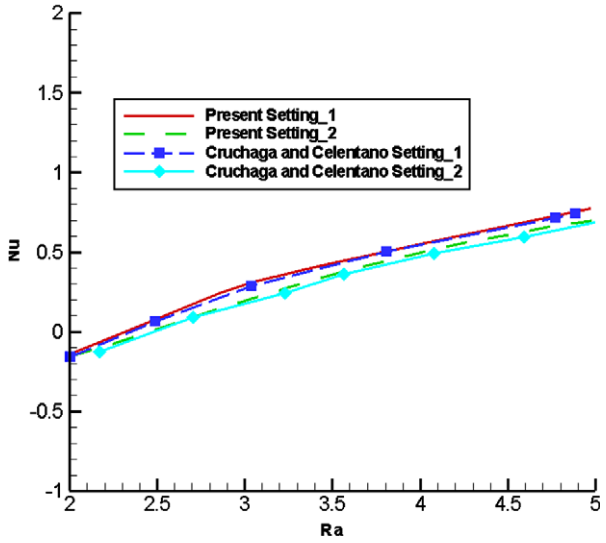

Fig. 16. Comparison for average Nu in vertical channel with two rectangular obstructions.

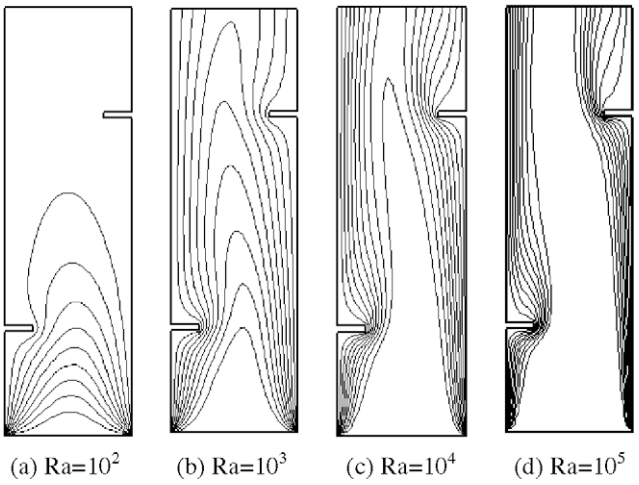

Fig. 17. Isotherms for natural convection in vertical channel with two obstructions (setting 3).

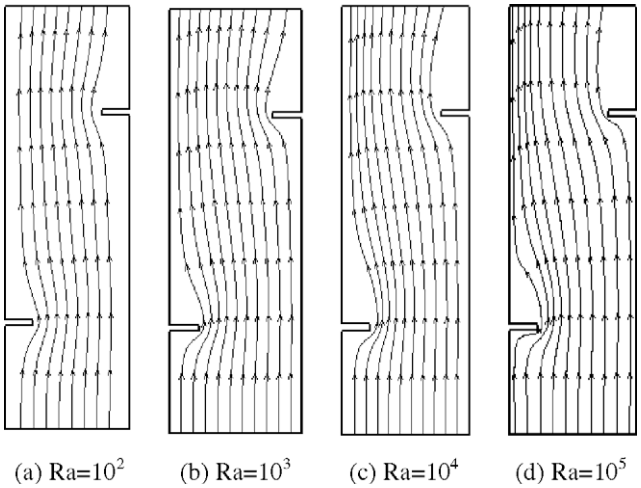

Fig. 18. Streamlines for natural convection in vertical channel with two obstructions (setting 3).

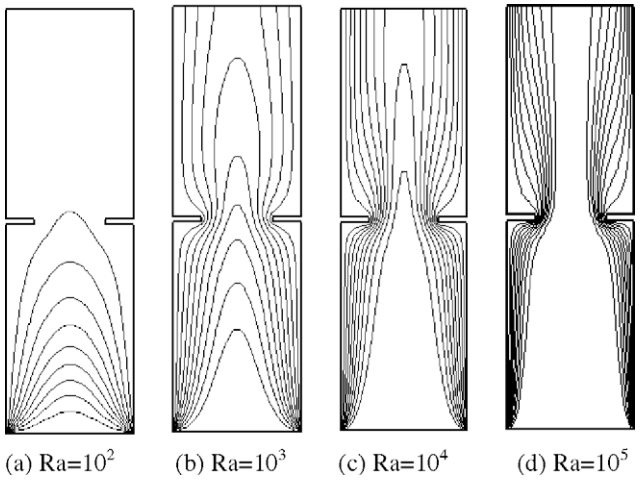

Fig. 19. Isotherms for natural convection in vertical channel with two obstructions (setting 4).

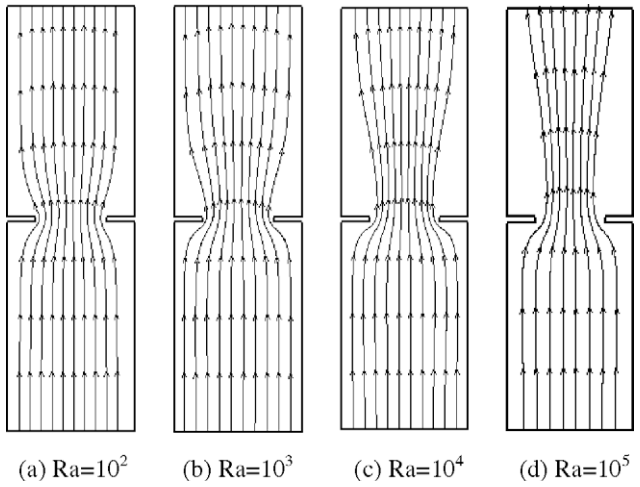

Fig. 20. Streamlines for natural convection in vertical channel with two obstructions (setting 4).

The average Nusselt number comparisons for vertical channels with aspect ratio 0.3 are shown in Fig. 21 with obstructions at different locations. Overall good agreement can be observed between the present average Nusselt number values and the computational results obtained by Cruchaga and Celentano [2].

5. Conclusions

Simulation results are obtained for natural convection with and without obstructions in a vertical channel. Effects of different Rayleigh numbers, obstruction locations and channel aspect ratios are investigated. The average Nusselt number along with thermal and fluid pattern for different test settings are presented. Results show that local heat transfer rates increase with the addition of obstructions for two reasons: (a) the increase of surface area, and (b) the flow accelerates around the obstruction regions. The heat transfer decreases with the enhancement of recirculation regions downstream of the obstacles. The overall heat transfer as well as the average Nusselt number increases with increasing Rayleigh numbers.

The employment of *h*-adaptation avoids the need for conducting mesh independent studies, which are required in most convection heat transfer studies. Meshes are refined in boundary layers

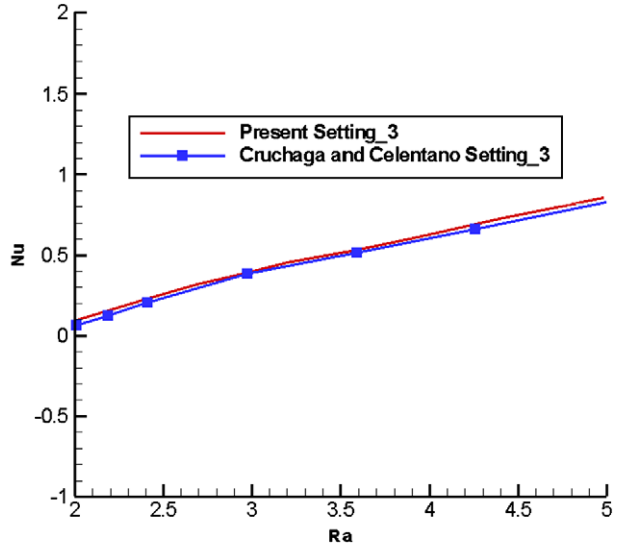

(a) Average Nu comparison for setting 3

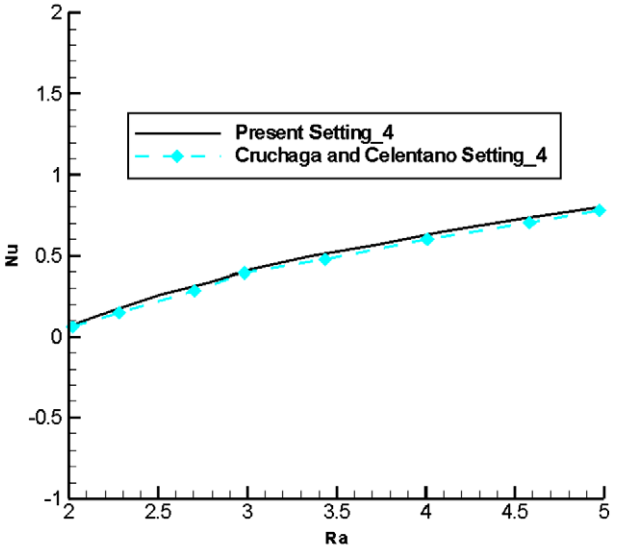

(a) Average Nu comparison for setting 4

Fig. 21. Comparison for average Nu in vertical channel with two rectangular.

and regions adjacent to obstructions, due to rapidly changing flow features and higher computational error. The use of adaptation is cost effective in the sense that refinement occurs only in local regions within the computational domain requiring increased mesh density.

Additional efforts are underway to examine much higher Rayleigh numbers and the onset of turbulence using the adaptive PFEM algorithm for natural convective flow in vertical channels with obstructions. In addition, the use of *hp*-adaptive PFEM to solve fluid flow and heat transfer problems especially shows promise for such problems. A preliminary three-step, *hp*-adaptive PFEM using a projection technique to account for pressure has been developed and tested using a simple class of fluid-thermal problems [13]. An *a posterior* error estimator based on the L_2 norm calculation is also used. The employment of a semi-implicit, time-stepping technique allows large time steps to be used for better stability while the explicit aspect of this method reduces storage requirements due to the use of condensed matrices.

References

[1] B.W. Webb, D.P. Hill, High Rayleigh number laminar natural convection in an asymmetrically heated vertical channel, J. Heat Transfer 111 (1989) 649–656.
[2] M. Cruchaga, D. Celentano, Modeling natural and mixed convection in obstructed channel, Int. J. Numer. Meth. Heat Fluid Flow 13 (1) (2003) 57–84.
[3] P. Viswatmula, M.R. Amin, Effects of multiple obstructions on natural convection heat transfer in vertical channels, Int. J. Heat Mass Transfer 38 (11) (1995) 2039–2046.
[4] R.A. Wirtz, R.J. Stutzman, Experiments on natural convection between vertical plates with symmetric heating, J. Heat Transfer 104 (1982) 501–507.
[5] S.A.M. Said, R.J. Krane, An analytical and experimental investigation of natural convection heat transfer in vertical channels with a single obstruction, Int. J. Heat Mass Transfer 33 (6) (1990) 1121–1134.
[6] T. Burch, T. Rhodes, S. Acharya, Laminar natural convection between finitely conducting vertical plates, Int. J. Heat Mass Transfer 28 (1985) 1173–1186.
[7] G. Desrayaud, A. Fichera, Laminar natural convection in a vertical isothermal channel with symmetric surface-mounted rectangular ribs, Int. J. Heat Transfer Fluid Flow 23 (2002) 519–529.
[8] Y.H. Hung, W.M. Shiau, Local steady-state natural convection heat transfer in vertical parallel plates with a two-dimensional rectangular rib, Int. J. Heat Mass Transfer 31 (6) (1988) 1279–1288.
[9] T. O'Meara, D. Poulikakos, Experiments on the cooling by natural convection of an array of vertical heated plates with constant heat flux, Int. J. Heat Transfer Fluid Flow 8 (4) (1987) 313–319.
[10] B. Ramaswamy, T.C. Jie, J.E. Akin, Semi-implicit and explicit finite element schemes for coupled fluid/thermal problems, Int. J. Numer. Meth. Eng. 34 (1992) 675–696.
[11] D.B. Spalding, A novel finite-difference formulation for differential expressions involving both first and second derivatives, Int. J. Numer. Meth. Eng. 4 (1972) 551.
[12] P. Nithiarasu, O.C. Zienkiewicz, Adaptive mesh generation for fluid mechanics problems, Int. J. Numer. Meth. Eng. 47 (1) (2000) 629–662.
[13] X. Wang, D.W. Pepper, Application of an hp-adaptive FEM for solving thermal flow problems, AIAA J. Thermal Phys. Heat Transfer 21 (1) (2007) 190–198.
[14] D.W. Pepper, X. Wang, A self-adapting model for assessing hazardous environmental releases, Nat. Hazards 44, 387–397.
[15] R. Moreno, Object-oriented implementation of the Galerkin Finite Element Method and its application to the numerical study of natural convective flows in enclosures, Ph.D. Dissertation, Rice University, 1997.
[16] S.V. Patankar, Numerical Heat Transfer and Fluid Flow, Taylor & Francis, 1980.
[17] D.K. Gartling, NACHOS – A Finite Element Computer Program for Incompressible Flow Problems. Part 1 – Theoretical Background, SAND 77-1333, Sandia Laboratories, Alguquerque, New Mexico, 1978.